Compact Readout Electronics for Position Sensitive Photomultiplier Tubes

Peter D. Olcott, Jonathon A. Talcott, *Student Member, IEEE*, Craig S. Levin, *Member, IEEE,* Frezghi Habte, *Member, IEEE, and* Angela M. K. Foudray*, IEEE, Student Member*

***Abstract*-- Two charge multiplexed readout schemes for Position Sensitive Photomultiplier Tubes (PSPMTs) have been developed and evaluated. A two-stage split-charge method is compared to standard positional charge division. The resulting electronic circuits are highly compact and will be initially incorporated into a small hand-held nuclear gamma ray imager for cancer staging. Electrical tests on the readout electronics are performed and intrinsic scintillation camera performance is evaluated using a 23x23 array of pixilated 2x2x3 mm^3 LSO crystals coupled to a H8500 flat-panel PSPMT.**

I. Introduction

Position-sensitive photomultiplier tubes (PSPMTs) convert scintillation light into a high gain current signal localized to group of anode segments. The current signal distribution contains important information regarding the energy, timing, and location of gamma ray interactions in the scintillatoin camera, which can be useful in both high resolution SPECT and PET applications. In this work, compact PSPMT electronics are designed, built and tested for a hand-held gamma camera for cancer staging [1]. In relatively large standalone systems that incorporate many relatively large PMTs, highly compact electronics is not crucial [2]. However, hand-held imaging systems require minimal electronic readout footprint and complexity [3]. The H8500 PSPMT has a 25 cm^2 field of view (FOV) using 8x8 anodes on a 6 mm pitch. It is challenging to multiplex a large number of anode analog signals into a practical imaging system. As a result traditional charge multiplexing techniques run into spatial non-uniformity issues.

In this work we use a compact flat-panel PSPMT (Hamamatsu H8500) and a lutetium oxyorthosilicate:Ce (LSO) scintillation crystal array for imaging low energy single photon emitters [4]. In our design we use an array of 2x2 mm^2 scintillation crystal pixels coupled to the PSPMT's 5.6x5.6 mm^2 anodes. We present a novel technique that combines two compatible charge-multiplexed position-sensing techniques.

A. Discretized Positioning Circuit (DPC)

Discretized position-sensitive readout circuits (DPC) [5] consist of a string or array of resistors that divide the charge between low impedance collection op-amps. The simple technique described provides positional charge division (see Fig. 1). The X and Y position can be determined by equations (1)-(2).

$$X_{position} = \frac{(V_a + V_b) - (V_c + V_d)}{V_a + V_c + V_b + V_d} \quad (1)$$

$$Y_{position} = \frac{(V_a + V_d) - (V_c + V_b)}{V_a + V_c + V_b + V_d} \quad (2)$$

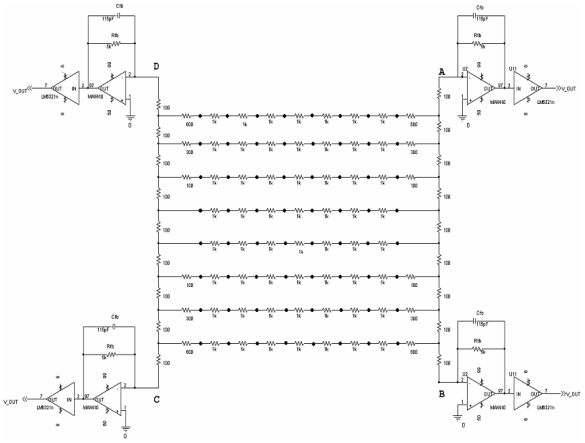

Fig. 1. A Conventional 2-D DPC network splits charge proportional to its Cartesian coordinates. This charge is collected on 4 charge sensitive preamplifiers named A, B, C, and D.

B. Symmetric charge division (SCD) Circuit

Instead of summing all the charge into a large resistive division network, a novel technique of dividing the charge into an X and Y decoder network is used [6]. The incoming charge is split in half, with one part being collected in a X collection op-amp, and the other half in a Y collection op-amp (see Fig. 2).

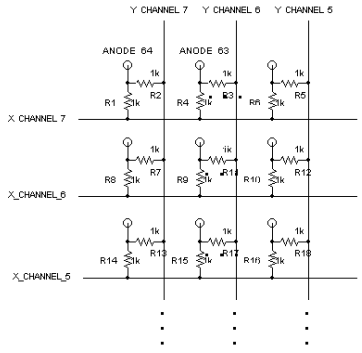

Fig. 2. Symmetric charge division replaces the conventional resistor divider scheme depicted in Fig. 1. At the end of each X or Y channel is a charge sensing preamp that collects and amplifies the charge proportional to its weight on the axis it encodes.

This novel technique which we will refer to as symmetric charge division (SCD) requires 16 amplifiers to collect the charge, one for each of the X rows and Y columns. For the H8500 flat-panel PSPMT, the position is encoded by

Manuscript received October 30, 2003.

Authors are with the VA Medical Center and the University of California San Diego (UCSD) School of Medicine, Department of Radiology, San Diego CA 92161 USA (telephone: 858-552-7511, e-mail: clevin@ucsd.edu).

determining the center of mass among the 8 channels along each row or column direction. The mismatch of charge deposited between X and Y paths are independent of each other. The drawback of this scheme is that it requires 2 * √N charge sensing preamplifiers for N anodes.

To reduce the number of channels from 16 to 4, a standard and very robust and technique [2] is used to encode the position along the axis as a current proportional to position (see Fig. 3). Because charge sensitive preamplifiers are used, a low impedance voltage is available. The voltage can be converted to a position by using a resistive division network. This method is superior to conventional resistive charge division (Fig. 1) because amplification is performed before division. The amplified signal is robust enough to divide into a current signal proportional to position.

The resistance on a row is determined by equation (3), where it weights each resistor proportional to its position on the axis. Gain is the amount of small signal gain from the output of the first level preamp to the output. n_{row} is the index of the of row, and $N_{channels}$ is the total number of channels per axis, in this case 8.

$$R_{row} = \frac{R_m}{\left[\frac{(n_{row}-1)*(Gain-1)}{(N_{channels}-1)}+1\right]} \tag{3}$$

After the two stages, the final position of an event is determined by equations (4) and (5). Fig. 4 shows a block diagram of the entire readout scheme proposed.

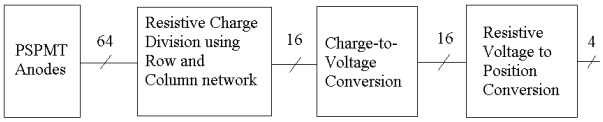

Fig. 3. Block diagram of newly proposed multi-anode interface

Comparing the position equations (4) and (5) to (1) and (2), we see that in the former the two output channels that encode X-axis are independent of the Y-axis and vice-versa. Also, the maximum voltage differences between any one channel compared to the other three is smaller in the proposed readout circuit. For example, if charge is injected in the corner of the resistor array, for the conventional design (Fig. 1), the voltage will be approximately 4 times larger than the average. On the other hand in the proposed SCD design (Figs. 3), the voltage will be only approximately 2 times larger than the average for an event on the corner.

$$X_{position} = \frac{V_{x+} - V_{x-}}{V_{x+} + V_{x-}} \tag{4}$$

$$Y_{position} = \frac{V_{y+} - V_{y-}}{V_{y+} + V_{y-}} \tag{5}$$

II. ELECTRICAL PERFORMANCE

A. Charge loss mechanism

There exists a path in the symmetric charge decoder for charge to be lost (see Fig. 4). First, the analysis of the impedance of virtual ground is critical in understanding this design limitation. An op-amp with an inverting feedback network comprising a capacitor C and resistor R in parallel operates as a charge sensing preamplifier. The time dependent output voltage, $V_{out,}$ to an impulse of current Q_{in} in the proposed circuit can be expressed as in equation (6):

$$V_{out}(t) \approx \frac{Q_{in}}{C}\left(1 - e^{-\frac{t}{RC}}\right) \tag{6}$$

The parallel combination of R and C can be expressed as the impedance Z. The impedance, a function of ω (frequency) looking into the virtual ground with an amplifier of finite gain A_0 and bandwidth ω_0 is given by equation (7):

$$R_{in}(\omega) \approx \|Z\| / \sqrt{\left[1 + \frac{A_0^2}{1 + \frac{\omega^2}{\omega_0^2}}\right]} \tag{7}$$

Because of thermal issues due to power consumption of the op-amp, the gain A_0 and bandwidth ω_0 to cannot be fully optimized to minimize R_{in}.

The 7 resistors and PSPMT anodes connected to each op-amp virtual ground form a parasitic path. Because a PSPMT anode is very close to an ideal current source, the charge splitting resistors connect the virtual grounds to each other. The charge from the anode after symmetric division is further divided by finite impedance, R_{in}, and the parasitic impedances of the other 7 preamps are a series combination of two charge splitting resistors and the finite impedances of the parasitic op-amps. The value of the charge splitting resistors must be large compared to effective R_{in} of the charge sensing preamp otherwise a large amount of charge will be lost, creating an offset voltage on unrelated preamps (see Fig. 5).

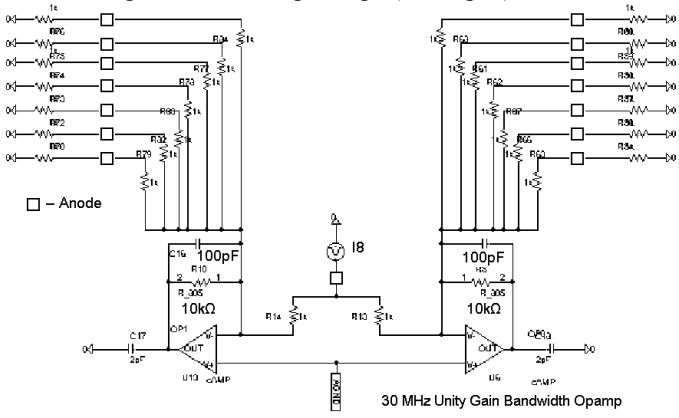

Fig. 4. A charge loss path exists from the anode to the virtual ground of the charge sensing preamp. In the example shown a charge source, I8, injects charge that is split symmetrically and collected by an X-axis and Y-axis preamp. Fourteen other anodes are connected to the same virtual ground and provide a path for charge to "leak".

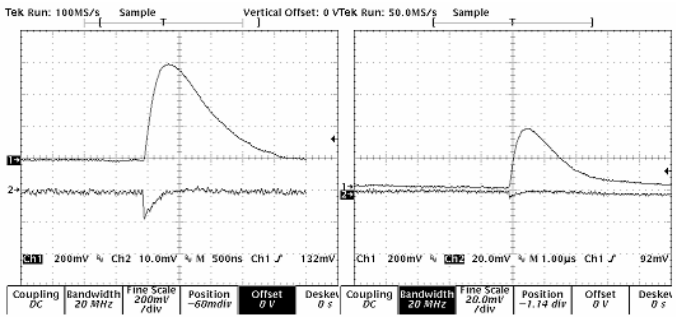

Fig. 5 In both digital sampling scope pulse captures, channel 1, the top trace, corresponds to the op-amp output in response to a impulse of current. Channel 2, the bottom trace, corresponds to the parasitic voltage step at the virtual ground due to finite impedance. The measurement on the left uses a 500ns decay constant for the feedback network Z, while the one on the right uses a 1µS time constant. The ratio of desired output to parasitic voltages is smaller for the latter case. Note the voltage scale for the right trace is a factor of two higher.

B. Spatial Linearity

To obtain spatial response using equations (1)-(4) for the DPC and PCD circuits, the four coaxial outputs of the front-end electronics are coupled to four spectroscopy amplifiers and a trigger system for use with a four-channel 12-bit 100ksps ADC board. The spectroscopy amplifiers perform Gaussian shaping with a 500 ns time constant. Both charge-multiplexed designs (DPC and SCD) were electrically probed to determine spatial linearity. The electrical probe consisted of a RC network designed to emulate the amount of charge and decay characteristics of an LSO pulse. The results are shown in Fig. 7. An approximate 100pC charge impulse with 40ns exponential decay time constant was used to test the entire positioning chain within both readout configurations. Comparing middle row linearity, each design performed within the tolerances of the passive components used and estimated by P-SPICE Monte-Carlo simulations of the designs before fabrication.

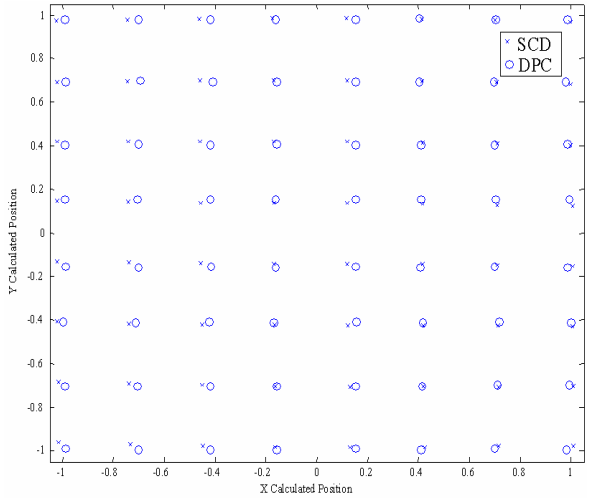

Fig.6. Each of the 64 inputs to the DPC and SCD circuits are electrically probed without the PSPMT and the position for both circuits is determined from a four-channel digitizer acquisition system and overlaid on the same plot.

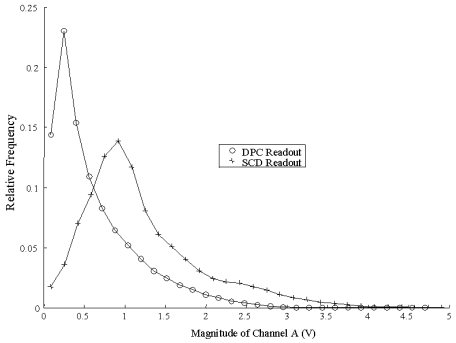

Fig. 7 The relative frequency of voltages for Channel A is shown for ^{57}Co flood irradiation. Selecting the worst-case event, usually at the corner, and comparing to the average voltage determines the peak to average.

Both designs showed excellent spatial linearity of less than 1% (see Table I). The DPC design performs slightly better due to the use of matched equal valued resistors. The SCD design is forced to use precise non-matched 1% resistors with a value based on equation (3).

The measured peak-to-average voltage shown in Fig. 7 confirms the large voltage difference observed between the two readout schemes. Due to voltage saturation, the gain of the preamp and processing chain must be able to accommodate the worst-case signals.

TABLE I
SUMMARY OF SPATIAL LINEARITY PERFORMANCE

Readout	RMS measured error	Peak-to-average voltage
DPC	0.52%	3.3
SCD	0.75%	2.4

For the same processing electronics the SCD design has a maximum voltage variation among the four readout channels of roughly a factor of two compared to over a factor of three for the DPC circuit (see Table I) in the current electrical setup.

III. FLOOD HISTOGRAM PERFORMANCE

The readout electronics plus the acquisition system were attached to the PSPMT coupled to a 23x23 array of 2x2x3 mm^3 LSO scintillation crystals. The crystals were polished on the one small face coupled to the PSPMT and the other faces of each crystal were "as cut". Each crystal was individually wrapped in two layers of white diffusely reflecting Teflon tape and then packed into the 23x23 array. The crystal array was directly coupled to the 2 mm thick glass window of the PSPMT without any additional light diffuser. The PSPMT has 49mm x 49mm of sensitive area. The 23x23 crystal array measured 50mm x 50mm with approximately a 2.1mm pitch in each direction. Thus, each of the crystals on the array perimeter had only roughly one quarter of their area coupled to the sensitive area of the PSPMT. Due to the small volume of the LSO crystals, the total measured background from ^{176}Lu was only ~400 cps for the 529 crystals (~0.76 cps/crystal) in a broad energy window from 50-400 keV.

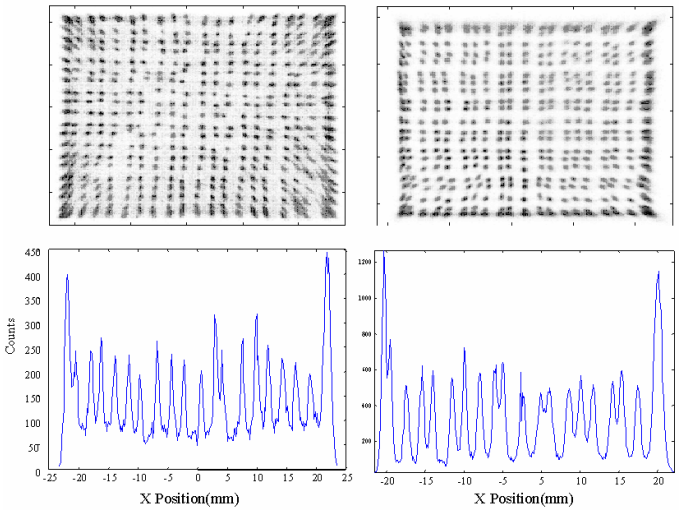

Fig. 8. Raw flood images of the LSO crystal array using the DPC(left) and SCD(right) readout with an open energy window are taken with a 100μC ^{57}Co source. The bottom two plots are middle row profiles through the flood image.

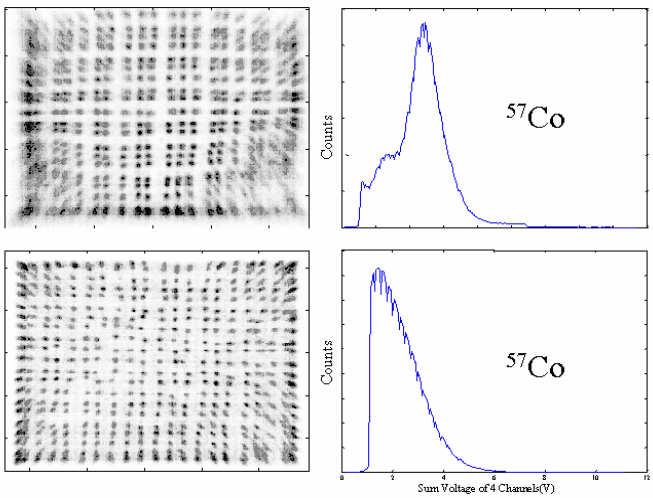

Fig. 9. Comparison of raw flood images between different gain settings for the DPC readout. Global sum energy spectra for the raw data are given on the right for each gain setting. The top image contains barrel distortion from compression artifacts created by the readout electronics, but a clear peak in the raw global energy spectrum can be seen. To avoid this saturation the amplifier gains are lowered considerably at the cost of the energy spectra as shown in the bottom row.

A. *Flood Irradiation*

The array was flooded by a 100μC ^{57}Co source at approximated 10cm from the center of the array. Approximately 1.9x10^4 events per second interacted with the crystal array and were detected by the acquisition system (see Fig. 8). Both readout schemes (DPC and SCD) were not able to resolve all 23x23 crystals in the array. For example, along the middle row profiles shown in Fig. 8, both schemes were only able to resolve 20 crystals out of 23. More than one crystal on each side mapped to the same location creating a hot edge artifact. This can be clearly seen in Fig. 8 on the edges of the middle row profile and around the perimeter of the flood images. The height of the last column in both middle row profiles show that approximately twice the number of counts are mapping to the edge. Since 20 crystals were resolved and the number of counts on the edge was only twice that of the crystals in the middle, it appears that an entire row of crystals was mapped to the adjacent crystal column on both sides of the array.

B. *Barrel Distortion in DPC Readout Scheme*

There is a clear tradeoff in a DPC readout scheme between spatial linearity and energy resolution. As can be seen in Fig. 10, good global energy resolution creates an image that has compression and saturation at the edges and in the corners. The poor performance can be traced back to the large peak-to-average voltage ratio (see Fig. 7 and Table I). A different choice in terminating resistors could change the peak-average voltage ratio restoring the spatial resolution, but there would be a tradeoff in signal gain and resulting dynamic range.

C. *Spatial Resolution*

Both readouts performed well in resolving the 2x2x3 mm^3 LSO array crystals spaced at 2.1 mm pitch. Spatial resolution was determined by the convolution between the spot size (0.7 mm) and the rectangular crystal size (2.0 mm) to about 2.6mm.

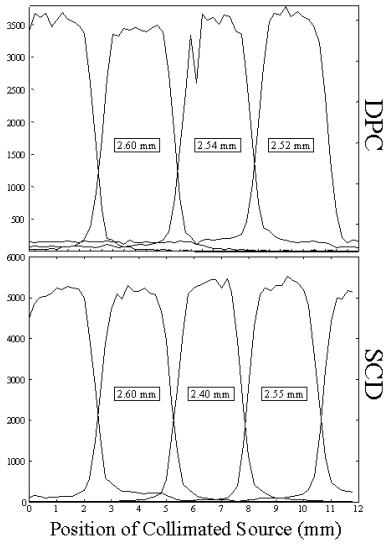

Fig. 10. Spatial resolution measured for DPC(top) and SCD(bottom) readouts with a collimated source that is stepped across array at 200μm intervals with a 0.7 mm spot size for a fixed time interval. Counts are binned to individual crystals and counted as a function of source position. FWHM are extracted from trapezoidal fits to the crystal profiles. Background radioactivity was low and was not subtracted for these measurements. Energy window was approximately 2 sigma around the 122 keV photopeak.

C. *Energy Resolution*

Energy resolutions were taken for 30 crystals from the 529-crystal array. The results are summarized in Table II. An individual energy spectrum was taken for each crystal by position gating based on the minimum distance to an identified peak. The resulting segmented image for the SDC readout is shown in Fig. 12 from which the individual crystal energy spectra were extracted. Fig. 11 shows an example of an average energy spectrum extracted from the same array crystal for the two readout schemes.

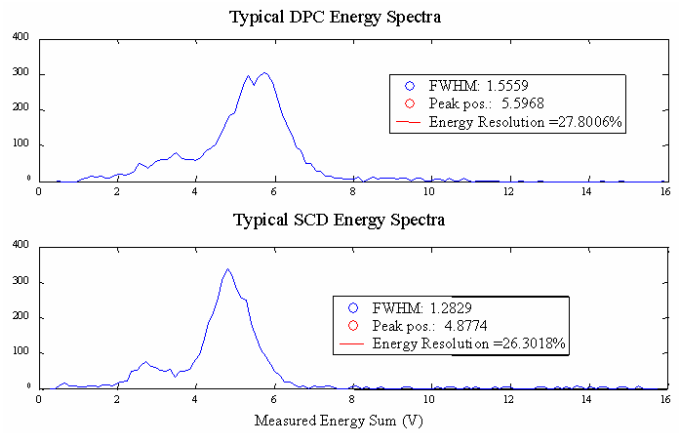

Fig. 11. Energy resolutions of a single position gated crystal from the large LSO crystal array taken from flood irradiation with a ^{57}Co source. In this measurement the DPC imager electronics were optimized for energy resolution rather than spatial linearity (Fig. 10).

The ~26% photopeak energy resolution value at 122 keV compares with the energy resolution measured by others [4] for ^{99m}Tc (140 keV photopeak) using 2x2x10 mm^3 LSO crystals. The small size of the crystal, 2x2x3 mm^2, relatively large PSPMT anodes (5.6x5.6 mm^2), and the absence of a significant light diffuser create a large non-uniformity in the collected light energy.

TABLE II
ENERGY RESOLUTION PERFORMACE

Readout	Best Resolution	Average Resolution	Worst Resolution	Standard Deviation
DPC	25.96%	27.83%	30.55%	0.4974
SCD	24.87%	26.32%	27.98%	0.7608

On average the light from each event is shared among several anodes. Because each anode has a different gain, the variation in the anodes convolves with the light distribution to broaden the 122 keV energy peak. To confirm that the crystal size effects energy resolution, single much larger crystal of 2 mm x 3mm x 10mm was coupled sideways (3x10 mm face) to the PSPMT and an energy resolution of 21.85% was measured. Using single isolated crystals of 2x2x3 mm^2 LSO did not improve the energy resolution compared to that measured from individual crystals of an array, ruling out the possibility that light sharing or other crystal array artifacts have any significant effect on the measured energy resolution.

IV. SUMMARY AND CONCLUSION

We have developed and compared two compact charge multiplexing readout schemes for readout of a flat-panel PSPMT. Both readouts provide good spatial linearity and dynamic range, and good spatial and energy resolutions. The SCD technique avoids the compromise between spatial linearity and energy resolution inherent to the DPC design. Both readout schemes (DPC and SCD) can be further optimized to provide better energy resolution for this hand-held surgical application. It is important to have a scintillation crystal array that will focus light in a way that minimizes the variation in light collection, and allows edge crystals to be correctly positioned within the array. We are currently investigating NaI(Tl) arrays in hope that we can improve the energy resolution. From the crystal flood images acquired it seems possible that even smaller crystals with less than the 2x2 mm^2 cross-section used in this work may be resolved with the present readout schemes. Collimator and energy resolution optimization are being investigated in order to determine the limit of spatial resolution performance of this compact imaging system.

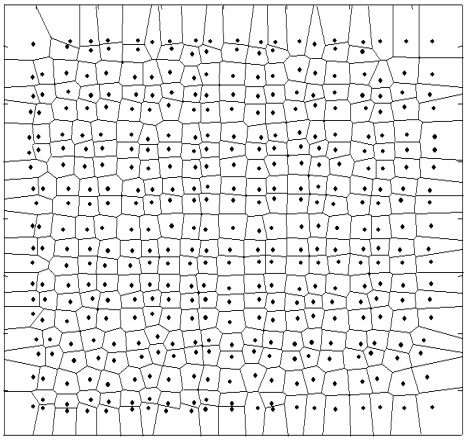

Fig. 12. Crystal map of the SCD imager is determined by selecting events that are the minimum distance to peaks identified in flood map.

V. ACKNOWLEDGMENT

This work was supported by a research grant (RG-01-0492) from the Whitaker Foundation. The authors would like to acknowledge PCB Express (http://www.pcbexpress.com/) for their donation of services for the fabrication of the PCB board. We acknowledge Don Johnson at UCSD CRMS, for his help in the fabrication of the fixtures for the spatial measurement and V. Popov for a very useful conversation related to the SCD readout.

VI. REFERENCES

[1] D. P. McElroy, E. J. Hoffman, L. MacDonald, et al, "Evaluation of performance of dedicated, compact scintillation cameras", Nuc. Sci. Symp. Conf. Rec., vol. 3, pp 21/109-21/113, 15-20 Oct. 2000

[2] D. R. Rollo, *Nuclear medicine physics, instrumentation, and agents,* Saint Louis, MO: The C. V. Mosby Company 1977, pp 232-237

[3] R. Pani, A. Soluri, R. Scafe, *et al*., "Multi-PSPMT Scintillation Camera", *IEEE Trans. Nucl. Sci.*, vol. 46, no. 3, pp 702-708, 1999

[4] Juan J. Vaquero, Jürgen Seidel, Stefan Siegel, *et al*., "Performance Characteristics of a Compact Position-Sensitive LSO Detector Module" *IEEE Trans. Nucl. Med. Imag.*, vol. 17, no. 6, pp. 967-978, 1998

[5] S. Siegel, S. R. Cherry, Y. Shao, "Simple charge division readouts for imaging scintillator arrays using a multi-channel PMT", *IEEE Trans. Nuc. Sci. Vol.43 No.3*, June 1996

[6] V. Popov, Thomas Jefferson National Accelerator Facility, private communication, 2002